Ionospheric Storms of Solar Cycle 24 and their Impact on the WAAS Ionospheric Threat Model

Lawrence Sparks, *Jet Propulsion Laboratory, California Institute of Technology*
Eric Altshuler, *Sequoia Research Corporation*

BIOGRAPHIES

Dr. Lawrence Sparks is a member of the Ionospheric and Atmospheric Remote Sensing Group in the Tracking Systems and Applications Section at NASA's Jet Propulsion Laboratory. He received his Ph.D. in Applied Physics from Cornell University and has pursued research in various fields including fusion plasma physics, solar magnetohydrodynamics, atmospheric spectroscopy, and ionospheric modeling. He is a member of the WAAS Integrity and Performance Panel and is currently working on issues concerning the impact of the ionosphere on satellite-based augmentation systems.

Dr. Eric Altshuler received his B.S. in mathematics and computer science from UCLA in 1989 and his Ph.D. in physics from University of California at Irvine in 1998. He is currently a Senior Engineer at Sequoia Research Corporation. He is a member of the WAAS Integrity and Performance Panel and is active in the development of ionospheric algorithms for WAAS. He has also worked on HMI analyses for the Multi-functional Satellite Augmentation System and for the SLS-4000 Ground Based Augmentation System.

ABSTRACT

Disturbances in the ionosphere can hinder the propagation of radio signals through the earth's atmosphere, thereby becoming major sources of error for position estimates determined from measurements of signals emitted by Global Positioning System (GPS) satellites. The Wide Area Augmentation System (WAAS) broadcasts parameters that allow a GPS user navigating over North America to compute corrections to position estimates and to bound the positioning errors that arise from ionospheric delay. Contributing the dominant term to the broadcast grid ionospheric vertical error (GIVE), the WAAS ionospheric threat model protects the user from threats posed by undersampled ionospheric irregularities. The threat model currently fielded has been derived entirely from historical observations recorded during solar cycle 23 when the WAAS receiver network was comprised of only twenty-five stations. The next upgrade of the WAAS ionospheric threat model will incorporate observations from solar cycle 24, recorded at all thirty-eight stations in the current receiver network. This paper examines the impact that solar cycle 24 storms are likely to have on both the threat model and on the consequent availability of the system, and it proposes a means of improving WAAS availability without sacrificing system integrity.

INTRODUCTION

Ionospheric storms are disturbances of the upper atmosphere that generate regions of enhanced electron density for time periods that may last up to several hours. Such storms can impede the propagation of satellite signals, thereby becoming major sources of positioning error for users of Global Navigation Satellite Systems (GNSS). To improve the accuracy and ensure the integrity of user position estimates derived from GNSS measurements, satellite-based augmentation systems (SBAS) have been implemented worldwide. The Wide Area Augmentation System (WAAS), operated by the United States' Federal Aviation Administration, is the augmentation of the Global Positioning System (GPS) providing assistance for aircraft navigation over North America. The WAAS *undersampled ionospheric irregularity threat model* [1][2][3][4][5][6] is a key constituent of the methodology that WAAS employs to protect its users from positioning error arising from the undersampling of ionospheric irregularities. The currently fielded threat model has been generated from historical observational data recorded by dual frequency receivers distributed over twenty-five sites across North America. The next upgrade of this threat model, to be fielded in the calendar year 2018, will incorporate observational data from the current expanded network of thirty-eight stations (see Fig. 1). This paper examines how ionospheric storms of the current solar cycle (solar cycle 24) will impact the WAAS ionospheric threat model and how this impact

will, in turn, affect WAAS availability. Since including more observational data in the construction of the threat model alone cannot have a positive impact on system availability, the next threat model upgrade can improve availability only if the methodology for threat model construction is modified. This paper concludes with a proposal to remove from the threat model, without adversely affecting system integrity, some of the threats that are currently retained in it, thereby enhancing system availability.

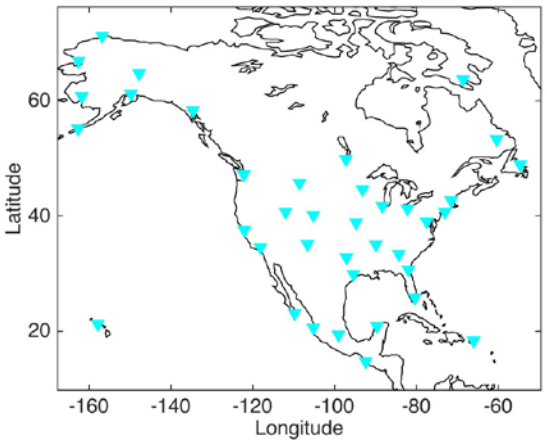

Figure 1. The current configuration of WAAS receiver station sites.

WAAS relies on geostationary satellites to broadcast correction messages that a WAAS-enabled GNSS receiver may use to determine a user's position and a safety-critical bound on positioning error due to ionospheric delay. These messages consist, in part, of a set of ionospheric grid delays (IGDs) and a corresponding set of grid ionospheric vertical errors (GIVEs) defined at regularly spaced ionospheric grid points (IGPs) over North America (see Fig. 2). Each IGD represents an estimate of the ionospheric delay that would be experienced by a signal propagating vertically above a given grid point. The broadcast GIVE at each IGP provides an integrity bound on the corresponding vertical delay estimate error. These delay estimates and integrity bounds are determined from fits of delay measurements recorded by the network of WAAS receivers [7].

Making the IGDs and GIVEs available to WAAS users as often as possible is a critical objective of WAAS. For each WAAS user, the broadcast GIVEs contribute to the computation of a horizontal protection limit (HPL) and a vertical protection limit (VPL). WAAS becomes locally unavailable when the HPL or the VPL exceeds, respectively, the horizontal alert limit or the vertical alert limit associated with a given navigation mode and level of service [8]. The GIVE at each IGP is defined in terms of a standard normal (Gaussian) distribution designed to overbound the tails of the actual distribution of the residual error in vertical delay estimation at the IGP after an ionospheric correction has been applied [5]. This overbounding error variance can be expressed formally as the sum of two terms:

$$\tilde{\sigma}^2_{GIVE} \equiv \tilde{\sigma}^2_{IGP} + \sigma^2_{undersampled},$$

where $\tilde{\sigma}^2_{IGP}$ is an inflated value of the formal estimation error variance due to the presence of a well-sampled ionosphere, and $\sigma^2_{undersampled}$ is the augmentation of the inflated error variance that protects the user from undersampled irregularities. The value of $\sigma^2_{undersampled}$ is provided by the undersampled ionospheric irregularity threat model as a function of metrics that characterize the spatial distribution of the measurements that comprise the estimation fit [5].

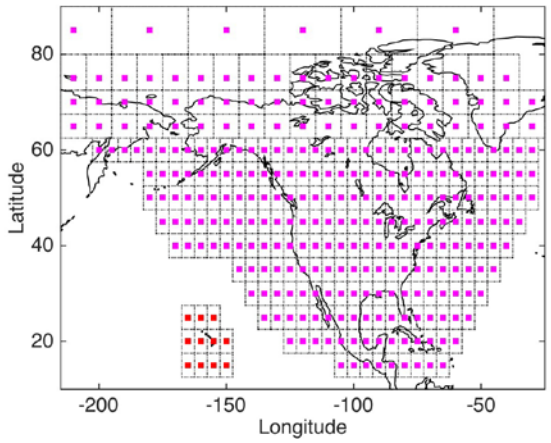

Figure 2. The WAAS ionospheric grid point mask. Magenta squares identify the IGPs in the IGP working set.

The WAAS ionospheric threat model is derived from fit residuals that occur when delay estimation is performed using sets of historical ionospheric data recorded under disturbed conditions. Since, at present, $\sigma_{undersampled}$ is the dominant term in the GIVE, the user's HPL and VPL (and consequently WAAS availability) depend critically upon the magnitudes of $\sigma_{undersampled}$ retrieved from the threat model.

The ionospheric threat model as currently fielded is derived from data collected during the largest storms of solar cycle 23 when, as noted above, the WAAS receiver network consisted of only twenty-five receiver stations. The next upgrade to this model will incorporate data from the current solar cycle, *i.e.*, solar cycle 24. The ionospheric storms that have occurred during this solar cycle have been much weaker in magnitude than the largest storms of the previous solar cycle. Nevertheless, storms in solar cycle 24 are expected to contribute critical points to the upgraded threat model, due, in part, to processing data from an increased number of WAAS

stations. Many of the additional stations are located in auroral regions of Alaska and Canada, providing measurement configurations that differ from those used to generate the current threat model.

New stations have also been added in Mexico. These, however, are not expected to contribute new critical points to the threat model, since the data analyzed in the construction of the current threat model included contributions from several Mexican receivers that were selected to mimic the geographic distribution of the new set of Mexican receivers. Since the overall level of ionospheric disturbance was much higher in solar cycle 23, the largest fit residuals (and the corresponding values of $\sigma_{undersampled}$) arising from data over Mexico in solar cycle 23 are likely to exceed in magnitude those of solar cycle 24.

This paper provides a status report on work in progress, namely, the generation of the next upgrade to the WAAS undersampled ionospheric irregularity threat model. The following section reviews the current methodology used to construct the threat model. In the subsequent section, we describe the projected impact that the storms of solar cycle 24 will have both on the ionospheric threat model and on WAAS availability, if the threat model methodology is not modified. This section includes a quantitative comparison of the magnitudes of the largest ionospheric storms in solar cycles 23 and 24. The comparison is based upon the storm magnitude metric used by WAAS to rank the relative strengths of ionospheric storms. The final section prior to the conclusion discusses the anticipated improvement in WAAS availability that may be achieved by a proposed modification of the threat model methodology – using the GIVE floor at each IGP to remove threats from the ionospheric threat model.

WAAS IONOSPHERIC THREAT MODEL METHODOLOGY

To construct the WAAS undersampled ionospheric irregularity threat model, delay estimation is conducted by fitting observations of slant delay under disturbed conditions to the standard thin-shell model of the ionospheric. The thin-shell model serves two useful purposes: (1) it allows us to associate with each slant delay measurement a unique point, the ionospheric pierce point (IPP), where the satellite-to-station raypath penetrates the model ionospheric shell; and (2) the ionospheric model provides a means of estimating the vertical delay at that IPP by multiplying the measured slant delay by a simple geometric factor.

A fit of vertical delay is performed at each IGP in the WAAS grid (the method of estimation, based upon a geo-statistical technique known as kriging, has been described elsewhere [7]), and a fit residual is generated for every measurement whose IPP lies within the *threat domain* of the IGP. The threat domain associated with an IGP is defined to be the grid cell centered on that IGP, *i.e.*, the set points that are closer to the given IGP than they are to any neighboring IGP (see Fig. 2). These fit residuals form the basis of the ionospheric threat model.

A fit residual associated with a delay estimate of the κ^{th} measurement is considered to be safely bounded when

$$\left|\bar{I}_\kappa - \tilde{I}_\kappa\right|^2 < K^2_{undersampled}\tilde{\sigma}^2_\kappa,$$

where $\bar{I}_\kappa$ is the measured slant delay of the κ^{th} measurement converted to vertical using the thin-shell model obliquity factor, $\tilde{I}_\kappa$ is the corresponding estimated value, $\tilde{\sigma}^2_\kappa$ is the inflated variance of the vertical delay estimate, and $K_{undersampled}$ determines an upper bound on the square of the residual in terms of the inflated formal error variance. In practice, $K_{undersampled}$ is set to a value of 5.33, and the shell for the computation of the obliquity factor is set by the *MOPS* [8] to 350 km, a representative height for the peak of the F2 layer of the ionosphere. For measurements whose IPPs lie within the threat domain of the IGP, the inequality is nearly always satisfied under nominal ionospheric conditions.

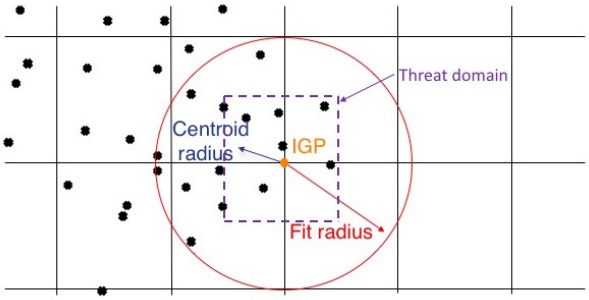

Figure 3. Schematic diagram of the fitting of vertical delay estimates to the thin shell model in the vicinity of an IGP.

Under disturbed conditions, however, the inequality may be violated. Each instance when this occurs is designated to be a *threat*. We define $\bar{\sigma}^2_{undersampled,\kappa}$ by requiring

$$\left|\bar{I}_\kappa - \tilde{I}_\kappa\right|^2 = K^2_{undersampled}\left[\tilde{\sigma}^2_\kappa + \bar{\sigma}^2_{undersampled,\kappa}\right].$$

Thus,

$$\bar{\sigma}^2_{undersampled,\kappa} \equiv \frac{\left|\bar{I}_\kappa - \tilde{I}_\kappa\right|^2}{K^2_{undersampled}} - \tilde{\sigma}^2_\kappa.$$

A threat exists whenever $\bar{\sigma}^2_{undersampled,\kappa}$ is positive, indicating that the inflated formal error of the regression is insufficiently large to bound all local ionospheric errors. At each IGP, we evaluate $\bar{\sigma}^2_{undersampled,\kappa}$ for every measurement whose ionospheric pierce point (IPP) resides in the IGP's threat domain. Threats are then tabulated as a function of two metrics (see Fig. 3) that characterize the distribution of IPPs around the fit center. The fit radius, R_{fit}, *i.e.*, the minimum radius of a circle centered on the fit IGP, encompassing all the IPPs in the fit, may be considered as a proxy for the density of IPPs: the smaller the fit radius, the larger the density, and the better the IPP coverage. The uniformity of the IPP coverage is quantified by the relative centroid metric (*RCM*), *i.e.*, the ratio of the centroid radius to the fit radius: *RCM* values near zero identify nearly uniform IPP coverage.

The tabulation of the raw data for the ionospheric threat model is performed according to the following equation:

$$\sigma^{raw}_{undersampled}(R_{fit}, RCM) = \max_{over\ \kappa,T} \sigma_{undersampled,\kappa}.$$

The maximization is performed over measurements κ and over a specified time interval T following each fit epoch, where T is 15 minutes. The time interval T accounts for GIVE computational latency, system broadcast latency, and message latency within the user receiver.

Threats are excluded from tabulation whenever a fit of slant delay measurements, converted to vertical delay, trips the local irregularity detector located at the fit center. The metric for this detector is based upon the standard χ^2 goodness-of-fit parameter associated with the vertical delay estimate – a diagnostic that has been found to scale reliably with the local level of ionospheric disturbance [7]. Only those threats are incorporated into the threat model where an ionospheric irregularity is present but not detected, due to undersampling, and consequently the local irregularity metric at the given IGP has not exceeded the trip threshold.

Threats are also excluded from the threat model when large-scale ionospheric disturbances have caused an *extreme storm detector* (ESD) to trip [9]. The ESD protects each user from the adverse impact of very localized regions of high electron density that have been found to occur during and after extreme storms, irregularities that might otherwise serve as sources of hazardously misleading information. When the ionospheric threat model is constructed, the ESD is used to exclude extreme storm events that might not be detected by the local irregularity detector. Excluding events for which the ESD has tripped serves to decrease the tabulated values of $\sigma_{undersampled}$, thereby reducing the broadcast GIVEs and improving WAAS availability under nominal ionospheric conditions.

The ESD relies upon a system-wide *ionospheric perturbation metric* (IPM), defined to be the maximum irregularity metric for all the IGPs in the IGP working set, *i.e.*, the IGPs at which IGDs and GIVEs are available to the user. The ESD trips when this metric has exceeded a high threshold value continuously for a required duration. In the system the tripping of the ESD effectively shuts down vertical guidance by WAAS for at least eight hours.

By introducing a *moderate storm detector* (MSD) [6], WAAS has recently made the ionospheric threat model dependent upon the regional level of ionospheric disturbance, splitting the threat model into two branches. Based upon the same ionospheric perturbation metric as the ESD, the MSD uses a similar algorithm as the ESD but with a lower disturbance detection threshold and a shorter confirmation interval. While the tabulation of the *disturbed-time branch* of the threat model excludes all threats arising from fits where either the local irregularity detector or the ESD has tripped, the tabulation of the *quiet-time branch* excludes, in addition, all threats where the MSD has tripped. Without these threats, the quiet-time branch of the threat model consists of smaller values of $\sigma_{undersampled}$, providing enhanced system availability whenever the ionosphere manifests quiet behavior. In the system the state of the MSD determines which branch of the ionospheric threat model is used to compute the GIVE at each IGP. Most of the time the MSD remains in an untripped state, and the quiet-time branch provides the values of $\sigma_{undersampled}$ used to evaluate the GIVE.

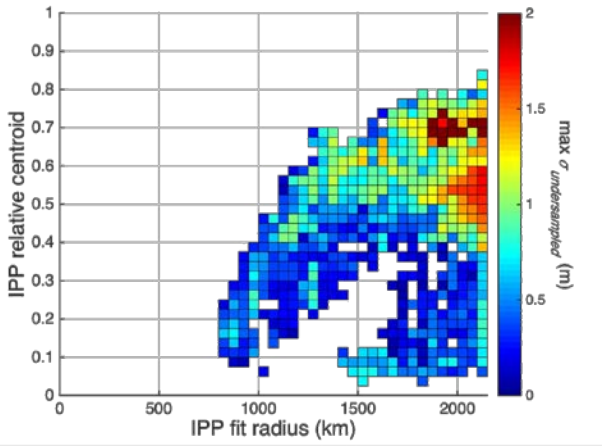

Figure 4. The raw data of the quiet-time branch of the ionospheric threat when the data processed are restricted to storm days in solar cycle 23.

Figure 4 displays the tabulated values of $\sigma^{raw}_{undersampled}$ for the quiet-time branch of the undersampled threat model when the data tabulated are restricted to storm days of

solar cycle 23. Note that here as in subsequent threat model plots the color bar scale is bounded at 2, causing all pixels with values greater than 2 to be colored brown. The computations have been performed using a software package developed at the Jet Propulsion Laboratory, entitled Ionospheric Slant TEC Analysis using GNSS-based Estimation (*IonoSTAGE*) [10]. The WAAS observations used to generate this branch consist of *supertruth* (version 4), a WAAS data set post-processed to provide a truth standard for ionospheric delay measurements [7]. This set of supertruth covers twenty-one days from the last solar cycle that include the most severe storms to have been observed. $\sigma^{raw}_{undersampled}$values in this branch are generated not only from fit residuals computed for sets of vertical delays drawn from the entire measurement set in each epoch, but also for sets where various fit measurements have been systematically excluded in the epoch – a technique known as data deprivation. By excluding observations in this manner, we effectively expand the historical data set in question and extend substantially the number of IPP configurations and their associated delay estimates represented in the threat model.

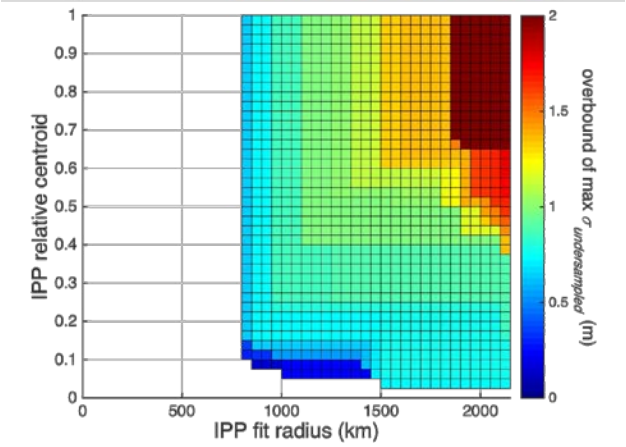

Figure 5. The quiet-time branch of the ionospheric threat when the data processed are restricted to storm days in solar cycle 23.

To construct from the raw data the tables of values that constitute the two branches of the ionospheric threat model, a two-dimensional overbound is applied to each branch of the raw data to ensure that $\sigma_{undersampled}$ is monotonically increasing both as a function of fit radius and as a function of RCM (see Fig. 5).

THE IMPACT OF SOLAR CYCLE 24 STORMS

It is well known that the largest ionospheric storms of the current solar cycle have been much less severe than those of the previous solar cycle. To quantify the magnitudes of ionospheric storms, WAAS has devised a scalar metric based upon the temporal behavior of the ionospheric perturbation metric described above. The storm magnitude metric takes into account both the maximum instantaneous level of the ionospheric perturbation metric and the temporal duration of the disturbance at a given level [11].

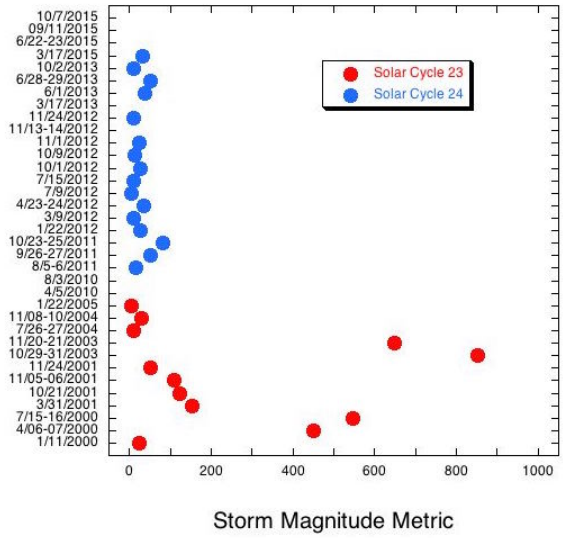

Figure 6. Storms in solar cycles 23 and 24 ranked according to the WAAS storm magnitude metric.

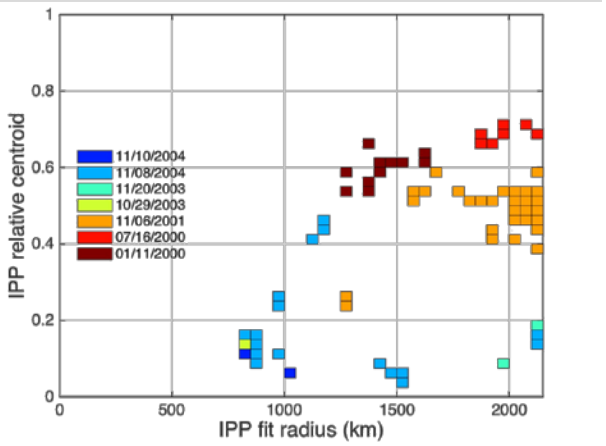

Figure 7. Critical points of the quiet-time branch of Fig. 5, colored coded to identify the storm day source.

Figure 6 shows how the magnitudes of major storms in each of the last two solar cycles rank according to the WAAS storm magnitude metric. The red dots identify the storms of solar cycle 23 whose data have been analyzed to produce the current threat model. The blue dots represent storms of solar cycle 24 where the geomagnetic K_p index attained the level of 7, indicating the presence of a moderate geomagnetic storm. To date, we have examined only storms that occurred prior to June of 2015. Note: had

we used the same criteria to select storms from solar cycle 23, many more red dots would appear.

The storm magnitude metric clearly differentiates known extreme storms, *e.g.*, the top four storms, from more moderate storms. No storm in solar cycle 24 has tripped the ESD. It might be expected that the tabulation of the ionospheric threat model would be dominated by fit residuals associated with the largest storms and that more moderate storms would exert little influence on the final values of $\sigma_{undersampled}$ generated. Since irregularity and storm detectors are used to eliminate the most extreme threats from the threat model, however, moderate storms can play a decisive role in determining the structure of each threat model branch.

We can partially assess the impact of moderate storms on the threat model by identifying the source of each *critical point* in a threat model branch. A critical point is a bin where the value of $\sigma_{undersampled}$ jumps to a larger value as either R_{fit} or *RCM* rises and crosses a bin boundary. For example, the quiet-time branch of the ionospheric threat model depicted in Fig. 5 is determined entirely by the set of critical points displayed in Fig. 6. In this latter figure, each of the critical points has been color-coded to identify the storm day responsible for the fit residual that has generated the corresponding maximum $\bar{\sigma}^2_{undersampled,\kappa}$ at the given fit radius and relative centroid metric. Note that while the extreme storms of 7/16/2000, 10/29/2003, and 11/20/2003 do each contribute critical points to the quiet-time branch of the threat model based entirely upon solar cycle 23 measurements, the more modest storms of 1/11/2000, 11/06/2001, 11/08-10/2004, contribute as well.

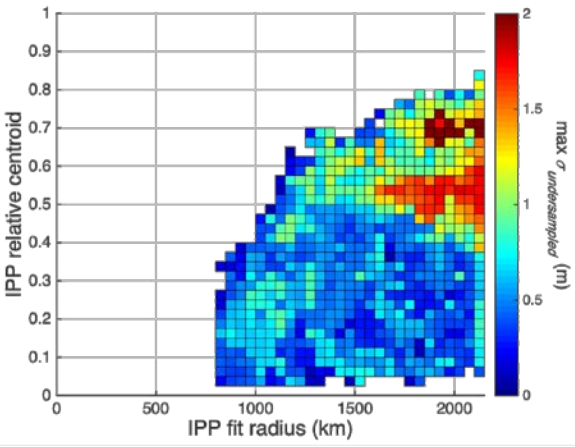

Figure 8. The raw data of the quiet-time branch of the ionospheric threat when the data processed include storm days from both solar cycles 23 and 24.

Incorporating threats from the storm days of solar cycle 24 depicted in Fig. 6 into the quiet-time branch of the threat model significantly alters the raw threat model data (see Fig. 8). Applying the overbound to these data produces the quiet-time threat model branch displayed in Fig. 9. Figure 10 shows the source of each critical point in a fashion similar to Fig. 7.

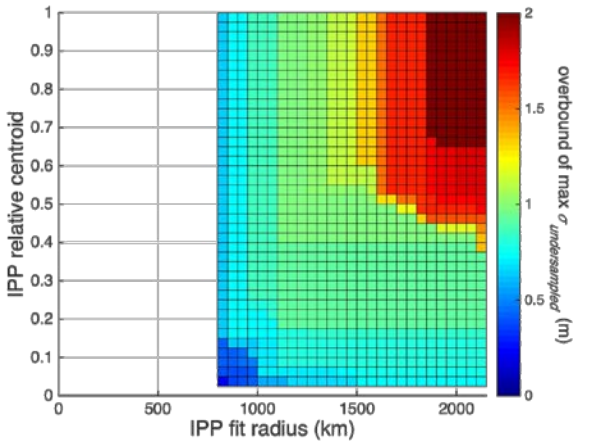

Figure 9. The quiet-time branch of the ionospheric threat when the data processed include storm days from both solar cycles 23 and 24.

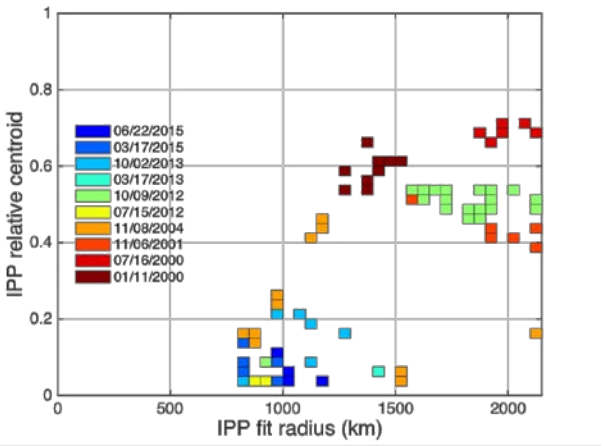

Figure 10. Critical points of the quiet-time branch of Fig. 9, colored coded to identify the storm day source.

If we compare Fig. 9 to Fig. 5, we find that the quiet-time branch of the ionospheric threat model has been considerably degraded, especially in the expanded region covered by red pixels. This degradation can be expected to have a negative impact on the availability of the system.

On a given day, availability can be evaluated by computing, at regular time intervals, the vertical and horizontal protection limits at user locations spanning the WAAS service area. The system becomes locally

unavailable, for example, when the irregularity detector at a nearby IGP trips and consequently, the system broadcasts the maximum GIVE value for that IGP, a GIVE of 45 meters, preventing any data at that IGP from being used for position determination. At any given user location, the availability will then be the fraction of the day that these protection levels did not exceed the corresponding alert limits. In Fig. 11 we plot contours of the availability for the LPV 200 level of service (with horizontal and vertical alert limits of 40 meters and 35 meters, respectively) on September 2, 2015, when GIVEs are computed using a threat model based entirely on solar cycle 23 data. September 2, 2015 is a day characterized by nominal ionospheric conditions.

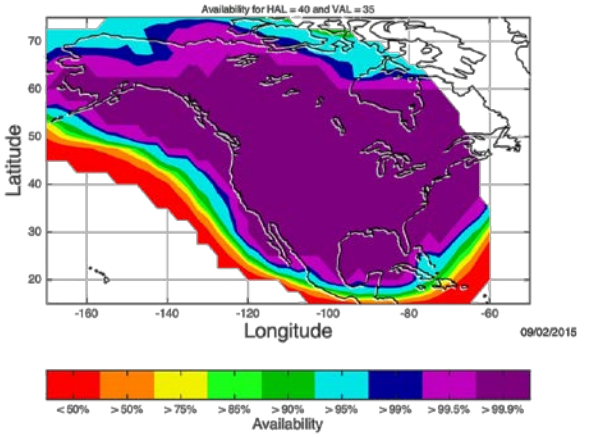

Figure 11. Contours of WAAS availability for the LPV 200 level of service on September 2, 2015, when GIVEs are computed using a threat model based upon only solar cycle 23 data.

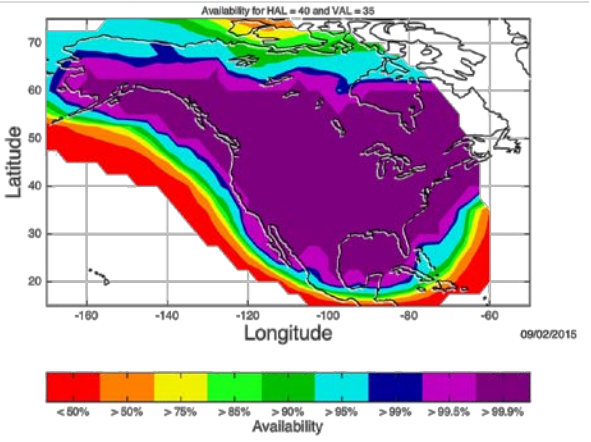

Figure 12. Contours of WAAS availability for the LPV 200 level of service on September 2, 2015, when GIVEs are computed using a threat model based upon solar cycle 23 and 24 data.

In the interior of North America, WAAS availability is nearly 100%. In this interior region, the sampling near a fit center tends to be dense and uniform, generating low values of the fit radius and the *RCM*. These values of the IPP distribution metrics identify relatively small values of $\sigma_{undersampled}$ in the quiet-time branch of the threat model. The lack of receiver sites beyond the eastern and western seacoasts, however, causes the IPP distribution around each fit center near a coast to become highly non-uniform, increasing the fit radius and *RCM*, and thereby increasing the values of the $\sigma_{undersampled}$ values used to compute GIVEs.

Figure 12 shows the results of computing availability using the same observational data but substituting the threat model based upon observations from both solar cycles 23 and 24. Note that the area of optimum coverage has contracted. As expected, the degradation of the threat model has reduced system availability, especially along each coast. The reduction in availability along the coast of California is of particular concern.

While this change in availability may appear to be minor, even small reductions in availability can have large economic consequences for WAAS users. Thus, the Federal Aviation Administration is strongly motivated to preserve, if not enhance, the level of system availability when the ionospheric threat model is upgraded.

USING THE GIVE FLOOR TO REMOVE THREATS

Currently we are investigating a possible modification to the threat model algorithm which would improve availability without diminishing system integrity. The fundamental idea is to use the imposed floor in the broadcast GIVE to eliminate the tabulation of some threats that are currently included in the threat model.

The GIVEs that WAAS broadcasts are quantized for the user receiver ionospheric correction message as specified by the *MOPS* [8]. The computed GIVE at each IGP is rounded upward to the next larger quantized GIVE value. The maximum GIVE broadcast value ($GIVE_{MAX}$ = 45 meters) is considered to be safe under all monitored ionospheric conditions; therefore, any computed GIVE value that exceeds $GIVE_{MAX}$ is reset to $GIVE_{MAX}$. In a similar fashion, any computed GIVE that falls below a threshold value of $GIVE_{floor}$, specified at each IGP to be at least three meters, is reset to $GIVE_{floor}$. Restricting all GIVEs to values no smaller than three meters provides redundant protection from any threat that gives rise to a GIVE less than three meters. Thus we argue that threats covered by the three-meter floor may be safely removed from both branches of the threat model without harming WAAS integrity.

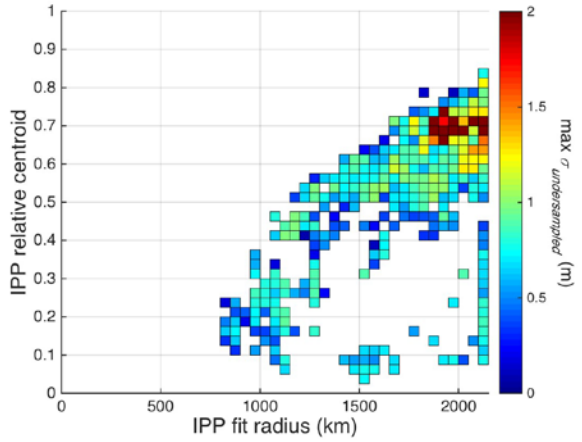

Figure 13. The raw data of the quiet-time branch of the ionospheric threat when the data processed include storm days from both solar cycles 23 and 24, where threats have been removed using the proposed GIVE floor logic.

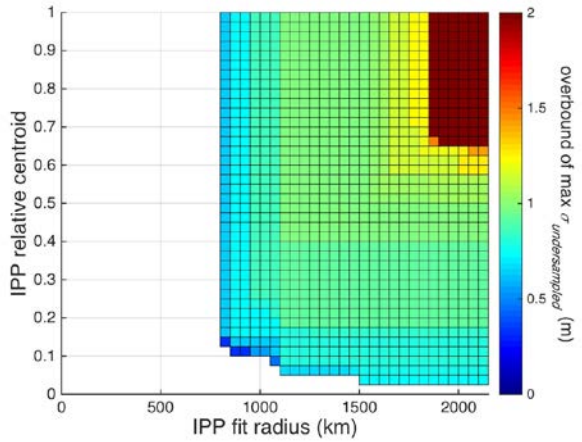

Figure 14. The quiet-time branch of the ionospheric threat when the data processed include storm days from both solar cycles 23 and 24, where threats have been removed using the proposed GIVE floor logic.

This is accomplished by imposing a new constraint on the threats to be tabulated in the threat model. In addition to requiring that $\bar{\sigma}^2_{undersampled,\kappa} > 0$, we now require

$$\tilde{\sigma}^2_{\kappa} + \bar{\sigma}^2_{undersampled,\kappa} > \tilde{\sigma}^2_{GIVE_{floor}},$$

which is equivalent to requiring

$$\left|\bar{I}_{\kappa} - \tilde{I}_{\kappa}\right|^2 > K^2_{undersampled}\tilde{\sigma}^2_{GIVE_{floor}}.$$

Combining the two conditions, we have a single condition for including threats in the threat mode:

$$\left|\bar{I}_{\kappa} - \tilde{I}_{\kappa}\right|^2 > K^2_{undersampled}\max(\tilde{\sigma}^2_{\kappa}, \tilde{\sigma}^2_{GIVE_{floor}}).$$

When we repeat the computation that produced Fig. 8 imposing this condition, the result we obtain is displayed in Fig. 13. By comparing to Fig. 8, it is clear that many threats have been removed, simply by the fact that there are now many (R_{fit}, *RCM*) pairs that are no longer associated with any threats.

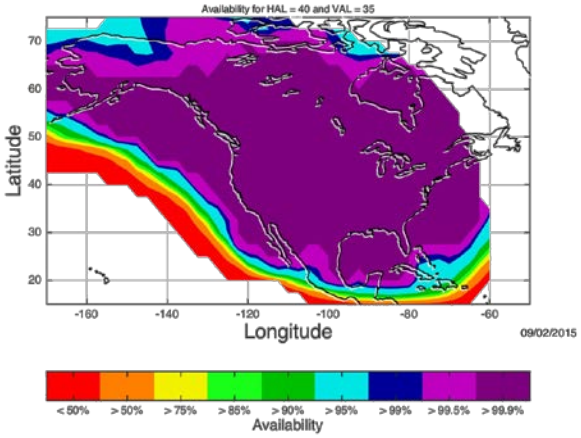

Figure 15. Contours of WAAS availability for the LPV 200 level of service on September 2, 2015, when GIVEs are computed using a threat model based upon solar cycle 23 and 24 data, where threats have been removed using the proposed GIVE floor logic.

Figure 14 shows the results of applying the overbound to the raw data of Fig. 13 to produce the quiet-time branch for the threat model that uses the GIVE floor algorithm. Figure 15 displays the availability achieved using the observational data of September 2, 2015, but substituting this new threat model. Note that availability improves not only with respect to that computed when the GIVE floor is not used to remove threats (Fig. 12); availability also improves with respect to that computed using data from solar cycle 23 only (Fig. 11). In particular, observe that the region of maximal availability along the coast of California has broadened significantly. By adopting the GIVE floor algorithm to remove threats, it should prove possible to improve both the integrity and availability in the new threat model upgrade.

CONCLUSION

This paper has reviewed the status of work-in-progress whose objective is to develop an upgrade to the WAAS ionospheric threat model, to be fielded in the calendar year 2018. Incorporating storm data from solar cycle 24 into the ionospheric threat model is projected to reduce WAAS availability if the current threat model methodology is not altered. To avoid this loss of availability, we have proposed modifying the algorithm that governs the construction of the threat model, introducing the use of the GIVE floor at each IGP to

remove threats that are currently included in the threat model. Based upon an analysis of solar cycle 24 observations recorded for storms up to June 2015, it is expected that the proposed changes in threat model methodology will result in enhanced WAAS availability without adversely affecting system integrity. It should be noted, however, that a full justification of this proposal consistent with the assumptions that underlie the current threat model algorithm has yet to be formulated.

ACKNOWLEDGMENTS

The research of Lawrence Sparks was performed at the Jet Propulsion Laboratory/California Institute of Technology under contract to the National Aeronautics and Space Administration and the Federal Aviation Administration. The research of Eric Altshuler was performed at the Sequoia Research Corporation under contract to Zeta Associates Incorporated and the Federal Aviation Administration.

REFERENCES

[1] Sparks, L., Pi, X., Mannucci, A. J., Walter, T., Blanch, J., Hansen, A., Enge, P., Altshuler, E., Fries, R., "The WAAS Ionospheric Threat Model," *Proc. of the International Beacon Satellite Symposium 2001*, Boston, MA, June 2001.

[2] Altshuler, E., Fries, R., Sparks, L., "The WAAS Ionospheric Spatial Threat Model," *Proc. of ION GPS 2001*, Institute of Navigation, Salt Lake City, UT, September 2001.

[3] Blanch, J., Walter, T., Enge, P., "Ionospheric Threat Model Methodology for WAAS," *Proc. of ION Annual Meeting 2001*, Institute of Navigation, Albuquerque, NM, June 2001.

[4] Paredes, E., Pandya, N., Sparks, L., Komjathy (2008), A., "Reconstructing the WAAS Undersampled Ionospheric Gradient Threat Model for the WAAS Expansion into Mexico," *Proceedings of the 21st International Technical Meeting of the Satellite Division of the Institute of Navigation (ION GNSS 2008)*, Savannah, GA, 1938-1947.

[5] Sparks, L., J. Blanch, and N. Pandya (2011), "Estimating ionospheric delay using kriging: 2. Impact on satellite-based augmentation system availability," **Radio Sci., 46**, RS0D22, doi:10.1029/2011RS004781.

[6] Sparks, L., and E. Altshuler (2014), "Improving WAAS Availability Along the Coast of California," Proceedings of the 27th International Technical Meeting of the Satellite Division of the Institute of Navigation ION GNSS+ 2014, Portland, OR, 3299-3311.

[7] Sparks, L., J. Blanch, and N. Pandya (2001), "Estimating ionospheric delay using kriging: 1. Methodology," **Radio Sci., 46**, RS0D21, doi:10.1029/2011RS004667.

[8] RTCA Special Committee 159, *Minimum Operational Performance Standards for Global Positioning System/Wide Area Augmentation System Airborne Equipment*, Doc. No. RTCA/DO-229D, RTCA, Inc., Washington, DC, December 13, 2006.

[9] Sparks, L., A. Komjathy, A.J. Mannucci, E. Altshuler, T. Walter and J. Blanch, M. Bakry El-Arini and R. Lejeune (2005), "Extreme Ionospheric Storms and Their Impact on WAAS," *Proceedings of the Ionospheric Effects Symposium 2005*, Alexandria VA.

[10] Sparks, L. (2013), "Ionospheric Slant TEC Analysis Using GNSS-based Estimation (*IonoSTAGE*)," JPL-D 34117, Jet Propulsion Laboratory, Pasadena, CA.

[11] Sparks, L., "Addressing the Effects of Space Weather on Airline Navigation", in *Guidance and Control 2012, Advances in the Astronautical Sciences*, Vol. 144, edited by Michael L. Osborne, *Proceedings of the 35th Annual Rocky Mountain Section Guidance and Control Conference of the American Astronautical Society*, Breckinridge, CO, February 3-8, 2012.